ISSN 2347-2251 www.iajpb.com
Vol. 21, Issue 3, Aug 2023

Indo-American Journal of Pharma and Bio Sciences

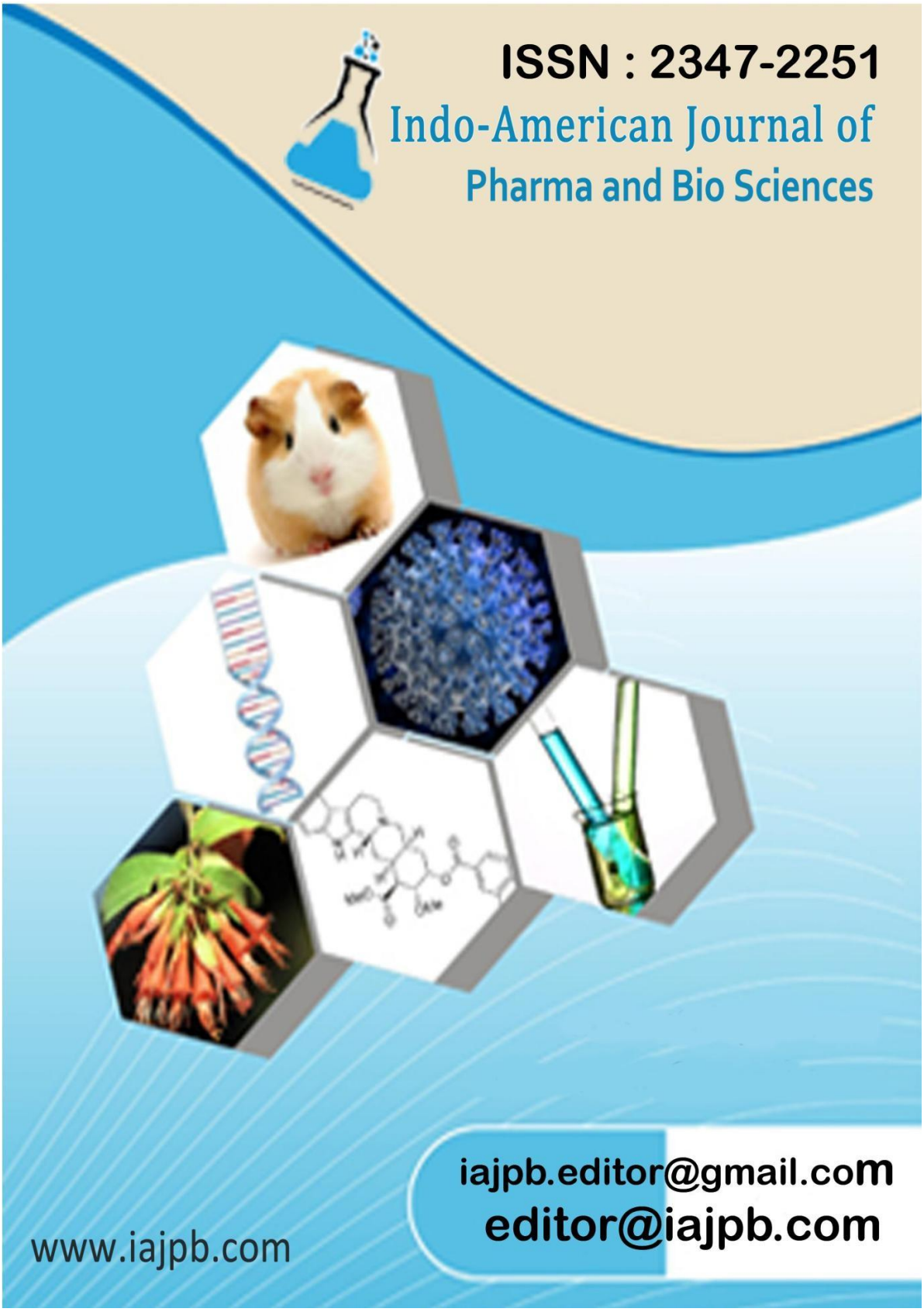

ISSN 2347-2251 www.iajpb.com
Vol. 21, Issue 3, Aug 2023

Indo-American Journal of Pharma and Bio Sciences

Contemporary Applications and Emerging Potential of Raman Spectroscopy in Cellular Lipid Profiling

K.Srikanth Kumar[1], J.Dharuman[2], G.Raveendra Babu[3], Mr R Srinivasan[4]

1. Associate Professor, Department of pharm.chemistry, QIS College of pharmacy, Ongole,AP
2. Associate Professor, Department of pharm.chemistry, QIS College of pharmacy,Ongole,AP
3. Professor, Department of pharm.Analysis, QIS College of pharmacy,Ongole,AP
4. Assistant Professor, Department of Pharm.AnalysisQIS College of pharmacy,Ongole,AP

ABSTRACT

The control of cell life processes is significantly influenced by lipids. Raman spectroscopy is a non-invasive approach that offers the comprehensive chemical composition of lipid profiles without requiring a complicated sample preparation process. It has higher promise in fundamental biology, clinical diagnostics, and disease treatment than other lipid detection techniques. The features and benefits of Raman-based methods were outlined in this review, along with their main use in illuminating cellular lipid metabolism.

*Corresponding author

K.Srikanth Kumar

srikanthk@gmail.com

1. Introduction

As significant biomolecular components, lipids have a role in the regulation of substance transport, energy metabolism, cell signaling, and cellular membrane architecture [1]. The development and advancement of atherosclerosis, diabetes, obesity, Alzheimer's disease, and cancer are all strongly linked to abnormal lipid metabolism [2,3]. Mass spectrometry (MS), fluorescence microscopy, and nuclear magnetic resonance (NMR) are the main conventional methods for identifying cell lipids (Fig.1). MS is often used to determine and measure the lipid content of cells. When combined with gas chromatography (GC) or liquid chromatography (LC), MS may provide comprehensive details on unsaturation levels, chain lengths, and lipid species [4]. However, in order to get high-quality and high-concentration samples, MS usually requires complex processes [5]. While precise information regarding lipid species could not be supplied, fluorescence microscopy uses specialized fluorescent dyes, such as Nile Red and BODIPY, to study the distribution and dynamics of lipid droplets (LDs) [6]. Furthermore, colorful signals that might disrupt lipids' regular function [7]. NMR provides a non-invasive way to investigate the chemistry and dynamics of lipids [8], but its inherent drawbacks include a comparatively poor sensitivity and significant sample preparation and experimental procedure requirements.

ISSN 2347-2251 www.iajpb.com
Vol. 21, Issue 3, Aug 2023
Indo-American Journal of Pharma and Bio Sciences

Approximately 1 in 107 dispersed photons transmit a part of their energy to the substance generating the scattering, a process known as Raman scattering (or inelastic scattering), first discovered by Indian scientist Chandrasekhara Venkata Raman in 1928. Rayleigh scattering, also known as elastic scattering, is the process by which a photon scatters without changing its energy. The Raman shift is the difference in energy before and after Raman scattering (DE). Anti-Stokes scattering happens when the frequency of the scattered light is greater (DE>0), while Stokes scattering happens when the frequency of the scattered light is lower than that of the incoming light (DE<0). Raman spectroscopy measures the Raman shift (usually expressed in wavenumbers, cm—1) based on the Raman scattering phenomenon. Raman spectroscopy, which works as a chemical fingerprint, gives details on a sample's chemical structure, composition, amount, crystal symmetry, and orientation [9] (Fig. 2). Raman is a label-free, nondestructive vibrational spectroscopy method that makes it easier to identify intracellular lipids without requiring complicated preparation or sample damage [9]. This article clarifies the several widely used Raman spectroscopy methods. utilized in biological

Indo-American Journal of Pharma and Bio Sciences

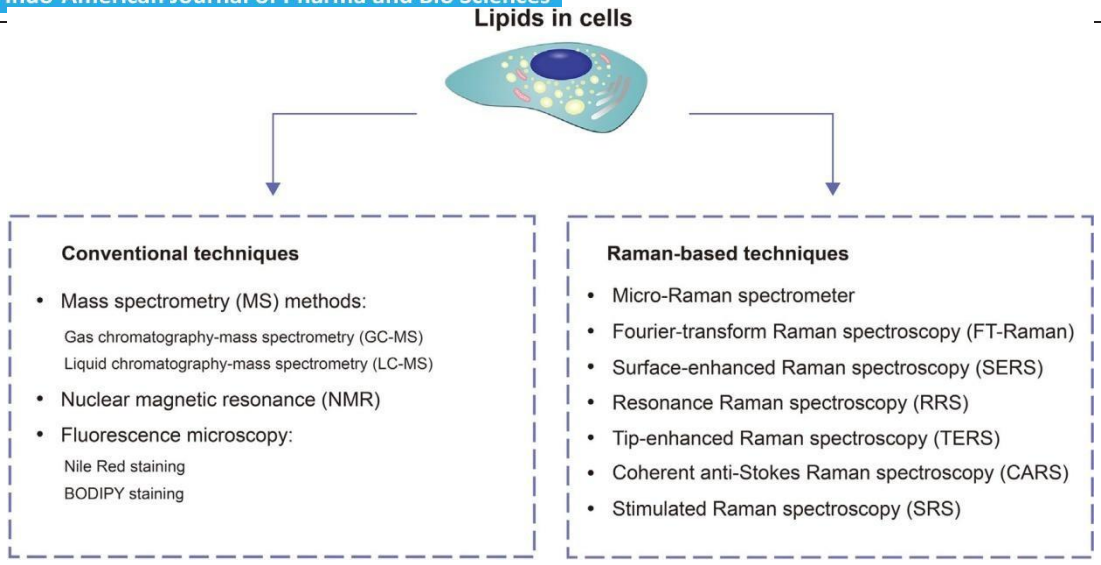

Fig.1.Schematicrepresentationofup-to-datetechniquestoidentifycellularlipidprofile.

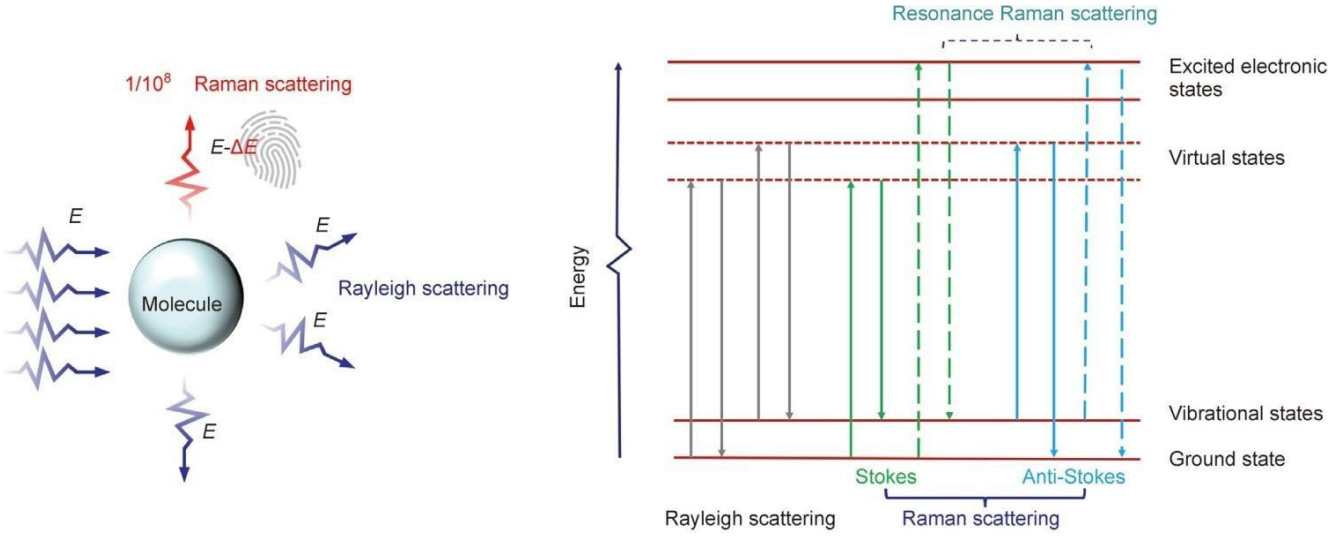

Fig.2.Principlesandenergy-leveldiagramsofRayleighscatteringandRamanscattering.

study and emphasizes their most recent uses in cellular lipid metabolism.

2. Using Raman-based methods as a lipid analysis tool High-resolution imaging and chemical analysis of materials are made easier by the micro-Raman spectrometer, which combines Raman spectroscopy with microscopy. The setup of an unusual laboratory micro-Raman spectrometer is seen in Fig. 3. After passing via filters and coupling optics, laser light enters the objective lens and is focussed onto the samples. The same objective lens then records the backscattered light from the samples, which is then sent to the spectrometer where a charge-coupled device (CCD) camera detects the light's dispersion into various wavelengths. Using Raman spectrometer software, raw data was transformed into Raman spectra and Ramanimages.

Fourier-transform methods and Raman spectroscopy are combined in Fourier-transform Raman spectroscopy (FT-Raman). The autofluorescence generated by excited lipids with visible lights was reduced when samples were stimulated by a 1,064 nm near-infrared (NIR) laser in FT-Raman but not by visible light [10]. According to reports, chemometrics and FT-Raman data may be used to distinguish between animal-originated feed samples and identify between diesel and biodiesel that have been adulterated with vegetable oils [11,12]. It is easier to distinguish glioblastoma

Indo-American Journal of Pharma and Bio Sciences
Vol. 21, Issue 3, Aug 2023

from meningiomas and other subtypes because to the distinctive lipid peaks 2,875 and 2,836 cm—1 that were detected by FT-Raman and correspond to CeH symmetric stretching vibrations [13]. Similar to ovarian cancer, lipid levels in platinum-resistant tissues are greater than in sensitive controls. It may be possible to distinguish between platinum-resistant and sensitive tissues using peaks resulting from lipid vibrations (2,817 and 1,714 cm—1) [14].

The low frequencies of NIR lasers cause the scattering signals of FT-Raman spectroscopy to be very weak since the intensity of Raman scattering is related to the fourth power of the excitation light frequency (n^4)[15]. The approximate mula for spatial resolution is d=0.61l/NA, where d is the solution limit, NA is the numerical aperture of the laser, and lislaser wavelength.

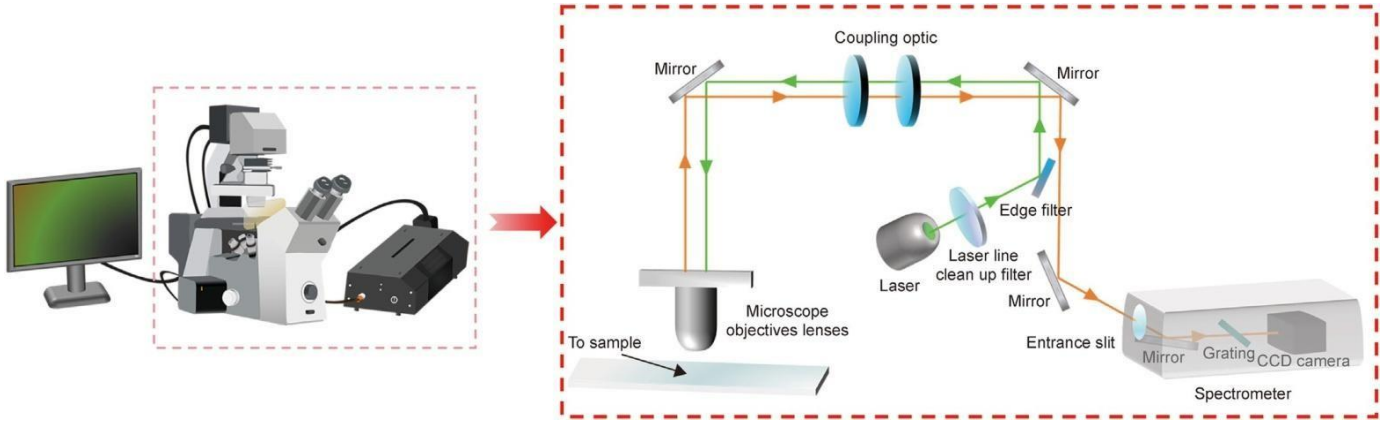

Fig.3.Typical laboratorymicro-Ramanspectrometer.CCD:charge-coupleddevice. objective lens), FT-Raman spectroscopy has a comparatively reduced spatial resolution [16].

By stimulating localized surface plasmons brought on by molecule adsorption on metal surfaces, colloids, or nanoparticles, surface-enhanced Ramanspectroscopy (SERS) dramatically increases signals in the 105–1010 range [17]. Thus, SERS demonstrated exceptional sensitivity and specificity, especially in identifying lipid-based disease biomarkers and monitoring drug delivery systems at low concentrations [18]. Qi et al. [19] successfully monitored the externalization of phosphatidylserine (PS) on the cell membrane during electrostimulation-induced apoptosis using micron-nano composites as SERS substrates and demonstrated the dynamic difference in PS externalization between tumor and normal cells. The impact of metal nanoparticles on liposomal characteristics, such as drug release and intracellular distribution, was investigated by Zhu et al. [20]. However, the interpretation of data becomes more challenging due to the low stability and repeatability of metal substrates [21].

When the excitation laser's frequency coincides (or nearly

corresponds to an electronic transition in the molecule under study, resonance Raman spectroscopy (RRS) is produced, and the signals are interpreted appropriately (Fig.1). Because of this amplification, the method is especially well-suited for identifying carotenoids [22,23], chlorophyll [22], and other colorful lipid molecules [22]. In the course of photosynthesis, the resonance Raman spectra of carotenoids and chlorophyll have been extensively studied [22]. According to the distinct Ramans scattering efficiencies of b-carotene and lycopener, respectively, at excitation wavelengths of 488 and 514.5 nm, and the prominent Raman peak that corresponds to the C]C vibration of the conjugate backbone of

Blume-Peytavietal. [24] discovered that oral supplementation with lycopene increased b-carotene and carotenoid molecules at 1,523

Indo-American Journal of Pharma and Bio Sciences
Vol. 21, Issue 3, Aug 2023

cm—1.

lycopen in human skin. The identification of molecules without unique electronic transitions is limited, particularly in the study of complicated clinical samples, since the complex and costly lasers matching electronic transitions of molecules are crucial points for RRS analysis [25].

Tip-enhanced Raman spectroscopy (TERS) is a sophisticated technique that combines Raman spectroscopy with scanning probe microscopy (such as atomic force microscopy, or AFM) to increase Raman signals around sharp metal tips made of copper, silver, or gold. The greatest advantage of TERS is its ability to perform spectroscopic analysis of lipids and nanoscale imaging [26]. However, since scanning probe microscopy requires relatively lengthy scanning periods, the method is also difficult to capture fast dynamic changes, including lipid rearrangement or transport, that occur on cellular membranes or subcellular structures [27]. TERS is commonly used in the analysis of substructures extracted from cells or located just below the cellular membrane and cellular processes with slower dynamic changes [27], but not 3D reconstruction for the highly limited lightfield near the tip apex. The intensity of TERS signals is also determined by the distance between the sample and probe as well as the shape of the probe, which also affects the system's stability and reliability. Forinstance,TERSidentifiedthecytochromecproteinstructuresinthemitochondria isolated from yeast cells, and typical phosphateresiduesoflipidmoleculesinthewave numberrangesof790e800

TERS technology was utilized for imaging and chemical characterization of newly synthesized

Because of the spatial resolution of less than 20 nm, phospholipids are found in the smooth endoplasmic reticulum (ER) in pre-adipocyte cells [29]. Furthermore, extracellular vesicles (EVs) produced from red blood cells (RBCs) may be identified by using TERS to analyze lipid membrane areas [30]. To get label-free structural imaging of dipalmitoylphosphatidylcholine (DPPC) monolayers supported on Au metal tips, Pandey et al. [31] first used TERS.

Two coherent excitation laser beams and a nonlinear interaction approach between two lasers and molecules are the fundamental techniques of coherent nonlinear Raman imaging, which includes coherent anti-Stokes Raman spectroscopy (CARS) and stimulated Raman spectroscopy (SRS) [32]. Because the CH2 stretching vibration in lipid acyl chains produces a very strong signal, CARS and SRS are ideally adapted to studying lipid molecules directly in vivo [32]. Unstained lipids, particularly concentrated vesicles such as cytosolic lipid droplets (LDs), in which the high signal intensity potentiates dynamic observation, could be imaged using CARS microscopy [33]. CARS microscopy was used once a week to image lipid structures in Caco-2 cells at the proper laser power settings (20e100 mW for the pump beam and 10e50 mW for the Stokes beam), and a significant increase in the quantity and size of LDs was noted during the 21-day cell culture period [34]. Image quality and detection sensitivity are inherently compromised by the non-resonant background that CARS signals display at the anti-Stokes frequency, which is independent of laser frequency tuning but related to the geometrical structure and local concentration of the object [32]. Additionally, CARS signals have a complex non-linear association with molecular concentration [32]. On the other hand, SRS microscopy overcomes the main obstacles of CARS. SRS signals are directly proportional to the analyte concentration and free from thenon-resonant

Indo-American Journal of Pharma and Bio Sciences

Vol. 21, Issue 3, Aug 2023

background, which is ideal for high-precision imaging and quantitative chemical analysis [35]. Lipids were primarily found in the intestinal tract, hypodermis, oocytes, and early-stage embryos of live Caenorhabditis elegans, according to SRS microscopy.

Quantitative analysis was used [36]. The cellular distribution of the CH2 and CH3 groups was recorded at 2,950 and 2,850 cm—1 [37] using SRS microscopy. These particular peaks were utilized to create high-resolution 3D imaging, and automated image processing methods were used to measure LD size, number,

as well as the spatial arrangement of individual cells [37]. According to the research, when exogenous oleic acid was added to non-adipocyte cells, including HeLa cells, lipid accumulation mostly happened as a result of a rise in LD numbers rather than size or lipid content [37]. Notwithstanding SRS's benefits, SRS microscopy has limitations in terms of detectability for low-concentration analytes, mainly because of its limited lase rexcitation power, which can be observed to surpass the damage threshold, and the interference from non-Raman background, which overpowers the true SRS signals in low-concentration conditions [35]. Taking into account the benefits and drawbacks of both CARS and SRS, researchers used both techniques as complementary analyses. Borek-Dorosz et al. [38] used CARS to study the distribution of lipids in endothelial cells.

based on the location of lipid peaks at 2,850 cm—1. Simul-

Concurrently, endogenous fatty acids (FAs) (at 2,930 and 2,850 cm—1) and exogenous deuterated palmitic acid (D-PA) (at 2,110 cm—1) were subcellularly localized by SRS imaging.

Therefore, it was investigated whether inflammatory endothelium cells could absorb exogenous saturated FA [38].

2. Cell sample preparation and Raman spectroscopic data reproducibility optimization

Fixed cells can be detected using Raman microscopy. Common fixatives include alcohols and aldehydes, which act by either breaking hydrophobic bonds in proteins or creating covalent bonds between proteins [39]. The cells were usually fixed for 4 to 15 minutes and then washed with phosphate-buffered saline (PBS) to get rid of any remaining fixative before analysis. Channetal [40] revealed differences in bandintensities associated to DNA, RNA, proteins, and lipid vibrations between unfixed or fixed normal and leukemia cells, suggesting that various fixation techniques may affect cellular Raman spectrum properties. In particular, unfixed and formaldehyde-fixed cancer cells reached an accuracy of up to 99%, but only 60% of methanol-fixed cancer cells were correctly diagnosed [40]. Furthermore, 4% paraformaldehyde (PFA) fixationcaused less modification in CARS signal and protein/lipid contentrelative to ethanolfixation, and retained LD morphology andprotein content similar to those of live cells [41]. Thus, 4% PFA is appropriate for cellular fixation in Raman investigation as it efficiently preserves cellular structure with no influence on lipids.

Additionally, Raman microscopy demonstrated notable benefits in life.

The unfixed adipocytes were imaged in PBS using CARSmicroscopy at a 785 nm laser, with incident laser powers of 62 mW (pump beam) and 6.5 mW (Stokes) [42]. The wavelength of the laser is typically used in live cell studies, which minimizes sample degradation and

Indo-American Journal of Pharma and Bio Sciences
Vol. 21 Issue 3, Aug 2023

photodamage even at higher powers and longer acquisition times. This is because cells can be imaged in PBS or cell culture medium without fixation due to the weak Raman intensity in a water medium [39]. When MIAPaCa-2 cells were imaged lipidically using CARS microscopy, the Stokes and pump beams were set at 1,040 and

The Raman shift was centered at 2,884 cm—1 at 800 nm, and a water immersion objective lens (40×, NA=0.8) was used.

to improve the laser beam's focus [43]. In order to facilitate the time-course monitoring of living cells, Raman spectrometers paired with a cell incubator were created [44].

The Raman substrate selection has a major impact on the quality and dependability of spectrum data and is essential for measuring cellular lipids. CaF2 and BaF2 are now the most often utilized substrates in bio-spectroscopy because they do not have distinctive Raman peaks in the 400–1,800 cm–1 cellular fingerprint spectrum [45]. The expensive cost of CaF2 significantly limited its use in the analysis of clinical samples, despite its low background signal and good optical transmittance. In comparison, glass and quartz substrates are more reasonably priced.

even if the comparatively large background radiation may partly obscure cellular biological signals. Suhito et al. [46] assessed several substrates, including quartz, silicate glass, and slide glass, for Raman analysis. There were peaks in the slide glass at 800 cm-1 that coincided with certain cellular lipid peaks within the range of

In contrast, silicate glass had substantial fluorescence interference [46] at 900e1,200 cm—1. Weaker substrate peaks were seen in quartz at around 600 cm—1 and 750—850 cm—1. Additionally, it was shown that stem cells and quartz substrates have high biocompatibility.

Quartz substrate proved appropriate for long-term monitoring of living cells using the Raman method, and cellular growth remained unaffected [46]. SERS analysis often uses metal substrates, such gold and silver, to identify low-abundance lipids. However, cellular viability may suffer as a result of metal ion leakage [18]. In order to replicate the extracellular matrix (ECM) environment, Gargotti et al. [47] examined HeLa and HaCaT cells grown on three distinct substrates: glass slides covered with rat tail collagen, CaF2 slides, and standard polystyrene cell culture plates. Compared to ordinary polystyrene plates and CaF2 substrate, collagen absorbs cell culture medium and disrupts the cellular cycle little, making it the perfect substrate for Raman spectrum measurements for a prolonged cell [47].

Reliable data is essential for identifying cellular lipids using

Raman analysis. First, control groups—such as the untreated group and the positive standard group—are necessary to guarantee the repeatability of the results. In order to confirm the accuracy of the experimental findings, these controls provide a positive or negative benchmark for further data analysis. While the results interpretation was validated by Raman spectra from the positive standard group to confirm the occurrence and relative concentration of specific lipids in the treatment group, the Raman spectral characteristics of the untreated control group were compared with those from the specific treatment group (e.g., drugs, staining) to acquire significant alterations related to the stimulation. Second, to reduce variability during sample preparation, experimental conditions, including cell source, cell density, treatment methods, and observation time, should be consistent. Thirdly, reference samples with known concentrations or commercially available Raman calibration

Indo-American Journal of Pharma and Bio Sciences

Vol. 21 Issue 3, Aug 2023

materials, such silicon wafers, should be used to calibrate the Ramanspectrometer prior to each experiment. Cali-bration using silicon wafers is essential to guarantee the instrument's

sensitivity and accuracy, resulting in a sharp and distinct Raman

521 cm—1 is the summit [48]. Additionally, it is advised to document the instrument's state and the surrounding circumstances throughout each

experiment because variations in temperature might produce changes in the Raman spectrum by altering the location and strength of peaks [49].

3. Key instruments and techniques for analyzing data in Raman spectroscopy

Raman spectroscopy may be used in a variety of contexts by quickly analyzing spectrum data and extracting pertinent information with the use of computer techniques [50]. Horiba Jobin Yvon, Renishaw, and Witec companies have all individually adopted commercial software, including LabSpec, Renishaw WiRE, and Witec [51e53]. MATLAB [55] and LabVIEW [56] are specialist bespoke software programs, whereas Origin, a popular graphing and data analysis program, also has a module for Raman analysis [54].

Normalization, denoising, and baseline correction are all part of the first data preparation, which helps to boost the

comparability and signal-to-noise ratio [53]. Using methods like spolynomial fitting and least squares, baseline correction reduces background signals [52]. Denoising utilizes techniques likeGaussianfiltering, meanfiltering, and Savitzky-Golayfiltering tosmooth the data [51]. Area and vector normalization are two examples of normalizing approaches that assist normalize the spectrum [50]. Peakfitting, which is done using Gaussian-Lorentzian or other methods, is an essential step for precisely determining peak locations, intensities, and widths as well as for separating overlapping peaks [57].

Accurate Raman chemical pictures of cells or tissue samples are often produced using sophisticated multivariate data processing techniques due to the intrinsic chemical complexity of biological materials. Principal component analysis (PCA) and clustering analysis are examples of unsupervised machine learning techniques that can handle data without labeled inputs. PCA processing identifies significant variation patterns in high-dimensional spectral data and helps distinguish the primary components of the analyte, such as PC1, PC2, and PC3, which stand for the largest, second-largest, and third-largest principal components, respectively [58]. This leads to the use of feature extraction and dimension reduction. PCA assists in identifying important changes in chemical bonds or composition in lipid analysis using Raman spectroscopy since it works under many situations.

Several immunophenotypes (CD45+/CD38+/CD138—and CD45—/CD38+/CD138+) in multiple myeloma samples were distinguished by combining Raman spectroscopy with PCA, and the spectral features recorded by PC1 and PC2 were mostly associated with protein.

and alterations in lipids [59]. By using PCA analysis, the algal cells under varying nitrogen stress durations were identified. This allowed for the formation of distinct clusters along PC1 (56%) and PC2 (26%), with b-carotene (1,521,1,161,1,152, and 1,001 cm—1) and chlorophyll (1,534 and 1,182 cm—1) serving

Indo-American Journal of Pharma and Bio Sciences
Vol. 21 Issue 3, Aug 2023

as the main discriminating pigments [60].
identifying samples with comparable spectral characteristics [61], such as distinguishing between healthy and cancerous cells [62]. In Raman spectroscopy, two clustering techniques are often employed: hierarchical cluster analysis (HCA) and k-means cluster analysis (KMCA). In order to successfully differentiate the LD content and distribution in different cell models, KMCA was used for multivariate analysis of SRS data by segmenting cellular images into distinct clusters that corresponded to different biochemical regions [63].HCAclustered the characteristic spectral data of calcifications in breast tissue captured by CARSmicroscopy, for example, 1,490

as well as 1,464 cm—1 for oxalate calcium connected to benign lesions and 961 cm—1 for phosphate calcium linked

to cancerous growths [64]. In order to identify possible pathological regions, the results are then mapped to create the spatial distribution of calcification types within the tissue [64]. Supervised machine learning, which includes partial least squares regression (PLS) and support vector machines (SVM), requires labeled data for training and prediction. PLS is used to create quantitative models that predict analyte concentration and provide accurate chemical composition [53]. PLS regression models on Raman imaging data showed that reduced glycoproteins and increased unsaturated fatty acids (UFAs) could be used as biomarkers to track the transformation of human-induced pluripotent stem cells (iPSCs) into cells that produce erythropoietin (EPO) [65]. In order to distinguish between several classes of multivariate data, SVM translates spectral data into high-dimensional space and looks for the best hyperplane [66]. Since radiation therapy clearly altered lipids and collagen in sensitive tumors while showing only slight alterations in resistant tumors, SVM was able to differentiate between radiation-sensitive and radiation-resistant tumor cells in the Raman spectra data [67]. Additionally, SVM was used to predict tumor radiation sensitivity before to therapy, which helped

the development of customized therapies [67]. During the subtype identification of acute lymphoblastic leukemia (ALL) using Raman spectroscopy, PCA showed the principally varied sources, PLS provided biochemical differences of cell types, and SVM optimized decision boundaries to obtain high specificity and sensitivity in the classification of ALL subtype [68]. This allowed for the effective extraction of valuable information from complex Raman spectral data by combining unsupervised and supervised learning methods.

4. Utilizing Raman spectroscopy to determine the lipid content of cells The cellular lipidome is mostly composed of FAs, triglycerides (TGs), phospholipids, sphingolipids, glycolipids, and cholesterol. The Raman scattering cross-sections of the lipids were influenced by their particular molecular structure and functional groups, particularly the lengthy non-polaracylchains, which are a crucial part of the structure [69]. The distinctive bands in lipid Raman spectra are intrinsically linked to the hydrocarbon chains seen in the fingerprint region. (between 500 and 2,000 cm—1). Specifically, CH2/CH3 vibrations, CH2twisting vibrations, and C—C stretching are all independently suggested by the 1,500–1,400, 1,300–1,250, and 1,200–1,050 cm—1 bands.
A frequent property of lipids is the spectral region between 2,900 and 2,800 cm—1, which is mostly associated with C—Hor=CH2/CH3 vibrations [69]. [69–71]. However, it is necessary to carefully evaluate interference with protein signals since proteins such as CH3 at 2,930 cm—1 also contain CeH stretching vibrations [70].
A long hydrocarbon chain that ends in a carboxyl group (—COOH) is the fundamental building block

Indo-American Journal of Pharma and Bio Sciences
Vol 21, Issue 3, Aug 2023

of FAs, a class of long-chain carboxylic acids. The degree of saturation (the amount of C]C) and the length of the carbon chain determine the chemical and physical properties of FAs [72]. The distinct spectral features of the cellular FAs' Raman spectra make them easy to identify. The most characteristic sites are around 1,500—1,400, 1,300, 1,180—1,060, and 890 cm—1. Stretching vibrations of C—C and C—O—Oskeletal vibrations, twisting vibrations of CH2, and deformation vibrations of CH2/CH3 may all be separately responsible for these [69]. Observed at about 1,656 cm—1, a prominent band resulting from the C]C stretching vibrations, and other features linked to =C—H stretching modes detected at approximately 3,015 cm—1 are among the notable distinctions between saturated fatty acids (SFAs) and UFAs [70,73]. These spectrum indicators provide vital information on the structural and functional impacts of FAs in cellular environments.

TGs serve primarily as cellular energy storage and are usually composed of a glycerol molecule esterified with three FA chains. When there is a greater need for energy, as occurs during prolonged activity or fasting, cellular TGs are broken down into glycerol and FAs. energy and material synthesis [74]. Each FA is connected to the glycerol's hydroxyl groups (—OH) via ester bonds. A peak at around 1,100 cm—1 resulting from C—O—C vibrations represents the glycerol backbone, while a peak at roughly 1,740 cm—1 resulting from C]O stretching vibrations represents esterlinkages [69,75]. Unsaturation in TGs was positively connected with the distinctive Raman peak ratio I1656/1444 [76]. Phospholipids, the primary lipids that comprise the structure of the cellular membrane, are typically composed of two FA chains, a phosphate group, a head group, and an aglycerol backbone. Among the several types that comprise the headgroup are choline, ethanolamine, serine, and inositol. The spectral signature of phospholipids is greatly influenced by the vibrations of the phosphatidyl moi-ety, with notable peaks often seen in the region of 1,096–1,080 cm—1. P—O and P]O-representing peaks All phospholipids have stretching vibrations inside the phosphate group; they are not unique to any one of them [69,77]. Furthermore, the molecular vibrations of choline N+(CH3)3 inphos-phatidylcholine (PC) resonate at 719 and 876 cm—1 [69,78]. The phosphatidylethanolamine (PE) spectra is characterized by the 760 cm—1 band that comes from the ethanolamine group [69]. Raman bands at 776, 576, 519, and 415 cm—1 reflect the isitol residue for phosphatidylinositol (PI) [79]. Like TGs, PS has characteristic peaks at 787, 733, 595, and 524 cm—1 that are associated with the glycerol [79]. Additionally, phospholipids showed ester and backbone linkages. The amide bond-linked FA, sphingosine backbone, and head group are used to distinguish between different types of sphingolipids [80]. Sphingomyelin (SM), an important kind of sphingo-lipid, is composed of the PC residue and ceramide backbone that link sphingosine and FA [79]. The amide bond between the acyl chain and the amino group of the sphingosine base is shown by the primary Ramanpeak for SM, which is caused by the amide I and is situated at around 1,643 cm—1. band [81]. Additionally, SM exhibits choline bands, which correspond to the characteristics of PC and are approximately located between 882 and 723 cm-1 [69].

Glycolipids consist of a lipid component, usually glycerol or sphingosine, and one or more hydrophilic sugar heads joined by glycosidic bonds. They may be divided into glycosphingolipids and glycoglycerolipids based on the lipid moiety. Cell identification, signal transmission, and cell-cell interactions all depend on glycolipids. With peaks at 1,163 cm^{-1} indicating asymmetric ring breathing of C—C and C—OeCglycosidiclink, 1,126 cm^{-1} for symmetric ring breathing of C—C and C—O—Cglycosidiclink, and 894 and 861 cm^{-1} for C—C and C—O—C1,4glycosidiclink, their characteristic Raman spectra are mainly derived from the sugar moiety [82]. Furthermore, as shown in SM [79], sphingoglycolipids also exhibit a noticeable amide band at 1,660 cm—1.

The four connected cycloalkane rings that make up the steroidal nucleus of cholesterol are often referred to as A, B, C, and D. The stiffness and planarity of cholesterol molecules are attributed to these rings. An integral part of cell membranes, cholesterol is crucial for regulating the stiffness and fluidity of membranes. By reducing phospholipid mobility at elevated temperatures, cholesterol stiffens membranes [83]. Furthermore, cholesterol preserves membrane mobility at lower temperatures by preventing phospholipids from grouping too closely together [84]. One end of different lipid components in complex biological objects [69]. After initially collecting SRS spectra of several lipid standards as calibration references, Xuet al. [87] successfully separated free cholesterol, saturated or unsaturated CE, and TG in liver tissue

ISSN 2347-2251 www.iajpb.com
Vol. 21, Issue 3, Aug 2023
Indo-American Journal of Pharma and Bio Sciences

sections using SRS spectral separation and linear least squares spectral decomposition techniques. Additionally, the spatial distribution of these lipids inside LDs was shown using typical peak imaging [87]. However, quantitative assessment of lipids may be achieved by comparing the intensity of the distinctive peaks with those of recognized lipid standard solutions. The SRS microscope captures lipid peaks at the designated Ramanband. 2,853 cm—1, and the volume percentage of the specific lipids is pro- The formula mass concentration=volume fraction×density, where density is a constant value for a certain lipid class (for example, the density of dioleoylphosphatidylcholin (DOPC) is 1.0101g/mL), is used to determine mass concentration after calibration and normalization operations. Furthermore, the altered lipid levels under a range of physiological situations were shown, including Madin-Darby canine kidney (MDCK) cells going through cellular senescence and brain tissues from models of Alzheimer's disease [88]. A review of the related characteristic peaks of cellular lipids is shown in Table 1. 5. Examining lipid dynamic alterations in LDs and cellular membranes using Raman imaging techniques

Lipids within cells may be readily recognized and mapped using Raman imaging technologies. Raman scattering has lately been used to develop microscopes such as SERS, CARS, SRS, and TERS [89]. By focusing a laser on each spot and scanning it point by point, Raman scattered light is captured at each site. Hyperspectral 2D or 3D imaging can visualize the spatial distribution of different lipids within cells by scanning across a single plane (typically the surface) to create a 2D Raman image, and scanning at different depths and stacking these layers to create a 3D Raman image. This is useful for in-depth analysis of lipid distribution, composition, and dynamics.
Table 1: Peaks of lipid features. OH is utilized to adorn cholesterol since it is a polar head group. This facilitates the formation of hydrogen bonds with the polar biomolecule. phospholipid molecular vibration Ramanband (cm—1) heads, resulting in the stability and integrity of the lipid bilayer [84]. This unique multicyclic structure is a significant feature, exhibiting particular Raman spectrum fingerprints at around 704 and 548 cm—1. [26,79]. LDs are very dynamic cellular organelles that alter in size, content, and quantity in response to energy demands in various cell types and even within the same cells at different periods [85]. LDs mostly come from the ER. Neutral lipids like TGs and cholesteryl esters (CEs) progressively build up in the inner leaflet of the ER membrane, creating a structure like a lens. The structures separate from the ER membrane during continuing growth, eventually becoming individual LDs encased in a monolayer of phospholipids [86]. The carbonyl stretching vibration is indicated by a significant band at around 1,740 cm—1, which is covered by the usual unsaturated TG signals in LDs' Raman profiles.

Indo-American Journal of Pharma and Bio Sciences

Table 1
Feature peaks of lipids.

Biomolecule assignment	Molecular vibration	Raman band (cm^{-1})
Lipids	C—H stretching, CH_2/CH_3 vibrations	3,010—2,800
	CH_2/CH_3 vibrations	1,500—1,400
	CH_2 twisting	1,300—1,250
	C—C stretching	1,200—1,050
UFAs	=C—H stretching	3,015
	C=C stretching	1,656
TGs	C=O stretching	1,740
	C—O—C vibrations of glycerol backbone	1,100
FAs/TGs	(C—O—O) skeletal vibrations	890
Phospholipids	P=O and P—O stretching	1,096—1,080
	$N^+(CH_3)_3$ symmetric stretching of PC	876, 719
	Serine residue of PS	787, 733, 595, 524
	Inositol residue of PI	776, 576, 519, 415
	Ethanolamine of PE	760
Sphingolipids	Amide I	1,643
	$N^+(CH_3)_3$ symmetric stretching of SM	882, 723
Glycolipids	Amide I of sphingoglycolipids	1,660
	C—C, C—O—C glycosidic link, asymmetric ring breathing	1,163
	C—C, C—O—C glycosidic link, symmetric ring breathing	1,126
	C—C, C—O—C 1,4 glycosidic link	894, 861
Cholesterol/CEs	Cholesterol ring vibrations	704
	β(CH2) in ringss	548
	C=O stretching of CEs	1,740

UFAs: unsaturated fatty acids; TGs: triglycerides; FAs: fatty acids; CEs: cholesteryl esters.

changes. Further insights into dynamic biological processes like lipid metabolism may be gained by using time-lapse Raman imaging to track changes in the distribution and composition of lipids over time. Here, we mostly discussed how Raman imaging is used to examine the primary lipid structures of LDs and plasma membranes. Increased LDs in tumor cells indicate improved invasion and metastasis capability [91], and there is mounting evidence that excess lipids stored in adipocytes and hepatocytes may cause insulin resistance and fatty liver disease [90]. Abnormal accumulation of LDs is linked to metabolic diseases and tumor development. A sophisticated method for evaluating the biological characteristics of LDs, such as their size, abun-dance, location, and form, is Raman imaging. Nenetal [92] used CARS imaging to investigate differentiated 3T3-L1 adipocytes and discovered Ramanshift at It is linked to the high density of C-H bonds in LDs at 2,845 cm—1. The patterns shown in Oil Red O staining, a comparison technique to verify the existence, size, and form of LDs, were quite similar to those seen in Raman photography of LDs. By using a Raman microscope, it was also possible to see the differentiation of human adipose-derived mesenchymal stem cells (hADMSCs) from nonexistent LDs to incidence and final formation of massive LDs [46]. The LDs in primary adipocytes have a higher degree of unsaturation, which generally corresponds to rising flexibility, while those in SVF-derived mature cells have a higher saturation, which correlates to more rigidity [71]. Primary adipocytes isolated from adiposet tissue exhibit more uniform and milder LD contours than stromal vascular fraction (SVF)-derived adipocytes. 3D imaging was used to get the displacement, speed, journey length, and directionality dynamics of LDs. using CARS, at 2,884 cm—1 corresponding to lipid CH2 vibrations microscopy [93]. A specific MATLAB-based program was developed throughout this procedure to examine important LD trajectory characteristics. Additionally, the particletracker plugin in Image J was added to monitor individual LD paths. Recent studies that used SRS to directly see tiny LDs and the whole dynamic process of LD synthesis have been emphasized. These studies showed real-time and three-dimensional monitoring of cellular LD movement and interactions with other organelles, including the mitochondria and ER [94]. Phospholipids that are integrated with proteins and cholesterol make up cell membranes. Lipid rafts are dynamic microdomains found in the cell membrane that are rich in saturated phospholipids, sphingolipids, and cholesterol. They are essential for lipid/protein sorting, cell adhesion, and signal transduction [95]. Raman provides label-free, non-invasive imaging of the chemical structure of cell membranes in contrast to optical imaging. The first full-spectrum of phase-separated lipid structural domains was identified by Opilik et al. [96] in 2011 using TERS for high-resolution imaging of lipid

Indo-American Journal of Pharma and Bio Sciences

Vol 21 Issue 3 Aug 2023

monolayers at the nanoscale with full spectral information at each pixel, which advances our knowledge of membrane structure and function. The molecular components of human pancreatic cancer cells (BxPC-3) have recently been visualized using label-free TERS imaging at a spatial resolution of about 2.5 nm [26]. This high spatial resolution offers great potential for revealing molecular characterization of complex biological samples and the distribution of biomolecules within different membrane domains, which contributes to the identification of composition and dynamic alteration within cell membranes. Additionally, TERS images were constructed without complex data processing but using the absolute intensity values of Raman marker bands, which improved efficiency [26]. CARS can do very sensitive quantitative analysis and show individual lipid bilayers. Phase-separated lipid domains in free-standing bilayers from giant unilamellar vesicles (GUVs) were studied by Potma et al. [97] using CARS, which removed geometrical constraints and produced a model that was quite similar to genuine cell membranes. They studied the distribution and phase separation of the membrane and specifically detected 1,2-distearoyl-sn-glycero-3-phosphocholine (DSPC) and the phospholipid DOPC. The imaging findings demonstrated that DOPC and DSPC form separate domains in the GUV membrane, with DSPC preferring to form gel phases and DOPC usually remaining in the liquid-disordered phase [97]. Images of cell membranes were acquired by CARS at the precise Ramanshift of 2,840 cm—1 in live HeLa cells to monitor the distribution of lipids and the progress of membrane repair [98]. In addition, the SERS was used to identify molecular components in RBC membranes that were in combination with silver nanostructures [99]. Similarly, high-resolution Raman imaging spectroscopy was used to discriminate between individual membrane lipids and deoxyribonucleoside triphosphates (dNTPs) inside living neural cells [100]. 2. Using Raman spectroscopy to study the lipids of various cell types Our attention now turns to the use of Raman spectroscopy in a variety of cell types, such as stem cells, adipocytes, and cancer cells, to illustrate cellular phenotypes/genotypes, cell differentiation, population composition, apoptosis, cell cycle, and metabolic processes, particularly lipid-related cellular functions, after describing the Raman spectroscopic characteristics of lipids and the fundamental role of Raman imaging in LD and cell membrane [101e103].

Stem cells The two types of stem cells—embryonic stem cells (ESCs) and somatic stem cells (SSCs)—are undifferentiated cells with pluripotency and the ability to self-renew [104]. ESCs, which are produced from the inner cell mass of blastocyst-stage embryos, have the capability for both significant proliferation and differentiation [105]. As an example, hematopoietic stem cells (HSCs) may develop into multiple blood cells [106], whereas SSCs present in particular tissues including bone marrow, adiposetissue, skin, and brain can differentiate into a restricted cell type relevant to their derived tissues [104]. Raman spectroscopy is helpful for assessing stem cell differentiation, quality, and consistency since it is non-destructive [107].
Since cellular energy generation and biosynthesis pathways control stem cell differentiation, Raman analysis of cellular nucleic acids, proteins, and lipids may reveal this transformation [108]. Human-induced pluripotent stem cells (hiPSCs) that have undergone differentiation considerably reduced nucleic acid bands (780 and 726 cm—1), but increased protein (1,660, 1,250, 1,030, and 1,003 cm—1) and lipid (1,440 and 1,295 cm—1) bands [108]. Raman imaging showed the change. by LDShallmark of adipocytes generated from adipose-derived stem cells (ADSCs) [46,48]. Early in the process (two days after induction), Raman microscope imaging identified bright areas around the cell nucleus that were suggestive of LD formation. Over the next few days, the shape of the LDs became bigger and rounder, and the intensities of lipid-related peaks were rose, with a noteworthy peak around 2,900 cm—1 [46], particularly at 3,013, 2,854, 2,727, 1,740, and 1,303 cm—1. Additionally, the area calculation value at 2,900 cm—1 peak compared to that at 2,935 cm—1 could be used to measure the differentiation of stem cells. procedure [46]. The hADMSCs were cultivated on a fibronectin-coated quartz substrate and stimulated to differentiate into adipocytes [109]. A 532 nm laser was directed at the live cells throughout the differentiation process, and the matching Raman spectrum was obtained. To evaluate the adipogenic potential, the distinctive peaks in the 2,850–2,855 cm–1 range that represent the concentration of LDs were measured [109]. HSC-derived neutrophils were grown on In order to obtain Raman spectrum data, gold mirror-coated glasses

Indo-American Journal of Pharma and Bio Sciences
Vol. 21 Issue 3, Aug 2023

were submerged in phenol-free RPMI1,640 solution. This resulted in a notable rise in lipid components, namely the cholinehead group (716 cm-1), but a reduction in signals linked to nucleic acids. Partialleastsquares discriminant analysis (PLS- With a classification error rate of 11.3%, the differentiation states were correctly predicted by the DA) model [110]. Ramanspectroscopy has also been used to identify different kinds of stem cells based on the cellular lipid compositions that are obtained [48]. Human embryonic stem cells (hESCs) and human mesenchymal stem cells (hMSCs) were shown to have lipid constitutions as early as 2010 [111]. Mouse ESCs exhibited increased spectral intensities at compared to induced pluripotent stem cells (iPSCs) at Stretching in UFAs, such as asarachidonicacid, docosahexaenoic acid, and linoleic acid, butlowerin- Saturated lipids have tensities at 1,445 cm—1 [112]. This contrast shows that ESCs have a larger amount of unsaturated lipids and reflectsthe dynamic changes in metabolism required for major keeping pluripotency in check. Using Raman spectroscopy, Simonoví´c et al. [113] observed the differentiation of stem cells originating from diverse dental tissues and discovered that all of the cells demonstrated fingerprint areas between 600 and 700 cm-1, as well as distinctive lipid peaks at 1,650 and 1,440 cm-1, might be used to differentiate several kinds. Bonemarrow-derived mesenchymal stem cells (BM-MSCs) obtained from healthy kid donors were identified using Raman by Kukolj et al. [114]. Although BM-MSCs from different origins have comparable Raman spectra, they may be different based on PCA analysis of proteins, nucleic acids, and lipids (1,450 cm—1CH2scissoring inlipids and 1,310 cm—1 C—H deformation of saturated lipids). In aberrant MSCs and hESCs, Harkness et al. [115] found elevated peak intensities at 1,300, 1,258, 1,196, and 1,158 cm—1, with peaks at 1,300 and 1,158 cm—1 ascribed to lipid-related structures.

Adipocytes

Differentiated from pluripotent stem cells, mature adipocytes are classified into three main types: white, brown, and beige adipocytes [117]. Adipocytes are essential for the control of energy metabolism, endocrine function, and thermogenesis [116]. Large LDs allow white adipocytes to store energy, and they also produce hormones like adiponectin and leptin to control systemic metabolism [117]. Smaller LDs and more mitochondria are characteristics of brown adipocytes, and their increased potential for thermogenesis is dependent on uncoupling protein 1 (UCP1), which is found in the inner membrane of the mitochondria [118]. A relatively novel kind of adipocyte, beige adipocytes are generated by cold exposure or exercise stimulus and usually appear inside white adipose tissue. Like brown adipocytes, they have several mitochondria and many tiny LDs, and they similarly release energy as heat [118]. Raman spectroscopy methods are used to examine characteristics of LDs in adipocytes. However, there is no significant correlation between LD diameter and unsaturation ratio [119]. Differentiated adipocytes from OP9 bonemarrow stromal cells under induced conditions (iOP9) exhibit larger LDs and higher unsaturation ratios, while spontaneously differentiated adipocytes (sOP9) display smaller LDs and lower unsaturation ratios.

The C-H band imaging of the LDS in 3T3-L1derived adipocytes revealed that micro-LDs (mLDs) first came from unspecific rather not from very nearby big central LDs areas, but rather from cytosol regions [120]. Additionally, research on the physical condition (acylchain order) and chemical makeup of particular LDs showed that freshly generated TGs were first deposited in tiny LDs rather than directly in the big LDs already found in adipocytes, and that LDs grew by "absorbing" the lipid content of smaller "donor" LDs. Importantly, lipid transfer across LDs took place over a period of hours, suggesting a carefully controlled process as opposed to a quick spontaneous fusion [121,122]. The degree of LD saturation in FAs-stimulated adipo- The intensity ratio of 1,660 cm—1 band (C]C stretching) to 1,450 cm—1 band (CH2 vibrations) reflected the cytes, and the unsatuFish oil (apolyunsaturated fatty acid, or PUFA) and oleic acid (a monounsaturated fatty acid, or MUFA) improved the ratio of LDs, but not stearic acid (an SFA) [123]. Special chemical bonds are introduced in the cell-silent Raman window (1,800—2,600 cm—1) using deuterium labeling techniques, enabling more accurate meta-tracking. bolic reactions of lipid molecules [124]. Pioneered by Kumar et al. [29] Nanoscale chemical mapping of freshly generated phospholipids in mouse pre-adipocytes pulsed with sodium deuterated stearic acid using TERS technology. Instead of aggregating into big clusters, these freshly created

Indo-American Journal of Pharma and Bio Sciences

Vol 21, Issue 3, Aug 2023

phospholipid molecules were probably going to form lengthy chain-like structures, according to the carbon-deuterium (C—D) bond's Raman scattering peak at 2,100 cm—1. An additional 9-hour research was conducted to monitor D-PA absorption in brown adipocytes and variations in CARSim- Ages at 2,100,1,741, and 1,655 cm—1 wavelengths were recorded, with peaks at 2,100 cm—1 revealing the intracellular distribution of TG and deuterated FAs [125]. Researchers then evaluated the C—D/C]O ratios, which show the amount of deuterated FAs. Brown adipocytes were shown to impede the absorption of D-PA in order to preserve unsaturated lipid homeostasis, as indicated by C]C/C]O (which indicates the degree of lipid unsaturation) for each LD [125]. The onset and progression of lipid metabolic illnesses may be more easily shown by the changes in lipid composition in adipocytes that are reflected by Raman spectroscopy. Confocal Raman spectroscopy was used to examine how high-glycemia (HG) affected adipogenesis in human visceral preadipocytes [126]. The distinctive peaks (2,970, 2,934, 2,895, and 2,852 cm—1) demonstrated that HGnot not only sped up adipogenesis but also changed the internal chemical composition of adipocytes, particularly the notable increases in the amount of LDSs, indicating that visceral fat might be a possible first location for metabolic disorders brought on by HG [126]. Raman study of the adipocytes in perivascular adiposetissue (PVAT) from young or old mice given HFD revealed that lipid unsaturation of adipocytes was decreased in the former, but young animals exhibited only slight alterations, suggesting that PVAT was vulnerable to HFD conditions as the mice aged [127]. Tumor necrosis factor (TNF) and D-PA-treated preadipocytes and adipocytes, respectively, may mimic the pathophysiological state of chronic inflammation and high-fat diet, respectively [128]. The production and development of LDs were similarly enhanced in mature adipocytes, although they were less noticeable than in preadipocytes. Preadipocytes sensitive to D-PA and TNF showed a large buildup of LDs but a reduction in lipid unsaturation [128]. However, there was little change in the quantity and make-up of LDs in primary adipocytes [128]. According to these results, inflammation and nutrition are important factors in obesity in the early phases of adipogenesis [128]. Cancerous cells Raman spectroscopy, when combined with chemometric techniques, revealed an increase in TG synthesis but a decrease of cholesterol in lung cancer cells (A549) when compared to normal bronchialepithelial cells (BEpiC). This allows for non-invasive lipid analysis in cancer cells, providing in-depth insights into tumor biology and metabolism.

markers(2,936,2,845,and1,444cm—1)forcancercells[129].A comparativeRamandatabetweenhigher invasiveM-4A4cellsandlower invasive NM-2C5 cells indicated that the M-4A4 cell linepossessedhigherpeakintensitiesat1,657and1,263cm—1(vibra-tionsofC]Cand=CH)thanthoseofNM-2C5cells,indicating ofthe elevated concentration of UFAs in M-4A4 cells [130]. Furthermore, the existence of numerous double bonds owing to polyunsaturated fatty acids (PUFAs) was inferred by the greater erintensity at 1,657 and 1,263 cm—1 compared to the value of 1,440 cm—1. Consequently, it was shown that PUFA content and cancer metastasis were correlated. Likewise, non-Using a machine-learning model based on spectral data of collagen and lipids, metastatic cancer cells 67NR were effectively separated from metastatic cancer cells FARN, 4T07, and 4T1 cells [55]. However, Raman imaging analysis could identify the genotypes of cancer cells. HeLa cells with cyclin-dependent kinase 6 (CDK6) gene knockout (KO) were distinguished from wild-type (WT) cells using Raman spectroscopy [70]. KO cells had a higher SFA content than WT cells. The Raman spectrum's SFAs/UFA band ratios (I1301/I1444, I1656/I2852, I1656/I3013, I2852/I3013, and I2930/I3013, etc.) were charac-known as Raman spectroscopic markers that may distinguish between WT and KO cells [70]. Furthermore, CH2 stretching vibration at 2,845 cm—1 shown by CARS revealed that the accumulated LDs were present in prominin-1 positive melanoma cells, however little LDs were seen in prominin-1 knockdown cells, indicating that

Prominin-1 promotes intracellular LD accumulation and regulates cellular lipid metabolism [131]. CARS and two-photonexcited fluorescence (TPEF) microscopy were used to examine the impact of CUB-domain-containing protein 1 (CDCP1) on lipid metabolism. It was found that CCP1 could decrease cytosolic LD abundance while increasing FAoxidation, which in turn drives triple-negative breast cancer (TNBC)

Indo-American Journal of Pharma and Bio Sciences
Vol 21 Issue 3 Aug 2023

metastasis [132]. As a tumor suppressor, the Von Hippel-Lindau (VHL) gene promotes the breakdown of hypoxia-inducible factor 1a (HIF1a). On the other hand, mutations in VHL hinder HIF1a degradation, which leads to the buildup of HIF1a and tumor formation [133]. Clear cell renal cell carcinoma (ccRCC) VHL-mutant tumor cells elevated CE-related peaks at 1,742cm—1,1,442cm—1, and702cm—1[134]. After the introduction of wild-type VHL gene, the number of LDs and CE levels were correlated with the VHL mutation. correspondingly decreased [134]. The use of Raman spectroscopy technology may reveal changes in lipid metabolism linked to the onset, spread, and treatment of cancer [135,136]. Rather than the makeup of LDs, the changed intensity of lipids may be the reason why X-ray radiation inhibits the growth of prostate cancer cells (PC3) [137]. MCF-10A cells showed a significant elevation of lipid content in comparison to human epidermal growth factor receptor 2 (HER2)-negative breast cancer cells. This was shown by the higher Ramanpeaks at 1,660, 1,338 and 1.BT474-LR cells with resistance to lapatinib, an Compared to sensitive BT474 cells, which were identified by the increased Raman peaks at 1,657,1,333, and 1,307 cm—1 [138], oral dualtyrosinekinase inhibitor had a higher phospholipid content. Jamieson et al. [139] assessed the effects of lipid-targeted drugs on PC3 cancer cells by comparing spectral bands from 2,800 to 3,100 cm—1. The altered lipid content of hormone-sensitive breast cancer cells and prostate cancer cells were especially manifested in LDs and SFAs amount by imaging lipid distribution and analyzing Raman data (2,800—3,015 and 830—1,800 cm—1) [140]. Oocytes, muscle cells, endothelium cells, and hepatocytes that have the capacity to store fat

Ramanspectroscopy exhibits broad applicability and flexibility in cell lipid research, especially in cells that have the capacity to store lipids under specified circumstances. Lipid storage is an essential cellular function that has a variety of effects on many cell types. Although LDs may provide energy and maintain blood lipid balance in hepatocytes [141], an inappropriate buildup of LDs can result in metabolic disorders such obesity and non-alcoholic fatty liver disease (NAFLD) [142]. The accumulation of LDs and their molecular properties in hepatocytes were effectively shown by Raman imaging [143]. By using CARS analysis, very low-density lipoprotein (VLDL) lipolysis products may cause a fast accumulation of LDs and an increase in UFAs in primary hepatocytes [144]. More esterified UFAs were produced to counteract the toxicity of SFAs, whereas co-stimulation with SFAs like palmitic acid and UFAs like solic acid and 13-hydroxyoctadecadienoic acid (13-HODE) raised the cellular saturated lipid content and saturation degree in the cores of LDs [144]. High concentrations of SFAs (palmitic and stearic acids) resulted in lower amounts of LDs and the induction of cellular apoptosis, according to Raman spectroscopy data of LDs in FAs-treated HepG2 cells [145]. Conversely, stimulation with soleic and linoleic acids led to higher accumulation of LDs, and cell death could be specifically triggered by linoleic acid but not oleic acid. Furthermore, oleic acid was formed from the FA chains of linoleic acid that entered the cells, indicating that the mechanism by which linoleic acid causes hepatocyte mortality may be different from that of SFAs [145]. Ma and colleagues [146] evaluated the viability of using Raman spectroscopy to detect human Using representative Raman biomarkers, such as 1,003 cm—1 of phenylalanine, 1,206 cm—1 of hydroxyproline, 1,744, 1,440, 1,300, and 1,080 cm—1 of lipids, and a two-layer Proliferating human hepatocytes were effectively distinguished from primary human hepatocytes (PHHs) using a machine-learning model. The presence of LDs in oocytes serves a crucial function in controlling cellular maturation and development, supplying the energy and structural elements required for early embryogenesis [147]. Additionally, recent research has shown a favorable association between the duration of embryonic diapause (ED) and the number of LDs [148]. An essential method for assessing the quality of oocytes and the viability of embryos before to implantation is Ramanspectroscopy.
in mammals. The protein-to-lipid ratio in oocytes was specifically determined by the ratio of peak intensities at lipid CeH deformation-related 1,447 cm—1 to phenylalanine-associated 1,605 cm—1, with a larger ratio being linked with high-quality development [149]. Okotrub's work on the label-free characterization of lipid phase transitions in frozen oocytes and embryos demonstrated the temperature-dependent evolution of LD phase states for the first time [150]. Lipid phase transitions in oocytes could be observed by Ramanspectroscopy, which helped to improve

Indo-American Journal of Pharma and Bio Sciences
Vol. 21, Issue 3, Aug 2023

cryopreservation techniques. In oocytes supplemented with stearic acid, cellular saturated lipids initially formed an ordered phase at the LD periphery. Upon warming post-cooling, a fraction of saturated lipids still remained in the ordered state, while mono-/poly-unsaturated lipids were redistributed to the LD core along with monounsaturated lipids. Their subsequent study with deuterated lipids revealed lipid phase separation in cryopreserved oocytes. moving to the ordered state below—10◦C [151]. Their most recent

According to study, chilling may cause pig oocytes' lipid phase status to change permanently [152]. Endothelial cells and other parenchymal cells may benefit from LDs' ability to buffer lipotoxicity and supply energy [153]. On the other hand, excessive lipid storage might harm vascular health by causing atherosclerosis and hypertension [154]. Three-dimensional observations of LDs creation inside endothelial cells were made using confocal Raman high-resolution imaging technology [155], as well as the process of LDs formation triggered by PUFAs [156,157]. According to the distinctive =C—D stretching mode bands (2,200—2,300 cm—1) of deuterium-labeled arachidonic acid (AA-d8), production in endothelial cells was verified [156]. The percentage of oleic acid and arachidonic acid in LDs was accurately calculated using Solver plu-gin, with oleic acid making up 80.6–91.3% of LDs and arachidonicacid ranging from 8.7%. to 19.4% in ex vivo vascular and cultured endothelial cells endothelial cells. It indicated that endothelial cells had the ability to release endogenous arachidonic acid and absorb exogenous oleic acid from the media [157]. Raman technology may thus be useful for monitoring the onset and course of a number of vascular illnesses [158]. Radwanetal. [159,160] examined (3S,3'S)-astaxanthin (AXT)'s potential as A new Raman probe was developed for the particular resonant Ramans scattering spectra at 1,520,1,159, and 1,009 cm—1, which made it possible to clearly identify lipid alterations in endothelial cells in a variety of arterial beds, such as the heart, brain, and aorta. AXT encapsulation with liposomes greatly increases endo- In TNF-a-treated endothelial cells, thelial cells, and free or encapsulated AXT not only reduced lipid unsaturation and LD numbers, but also had some anti-inflammatory properties [160]. LDs serve as energy stores in muscle cells during exercise, but aberrant lipid buildup in muscle cells interferes with energy consumption and is linked to muscular dystrophies and insulin resistance [161]. Here is a summary of the lipid properties of muscle cells as determined by Raman analysis. There were only slight changes in the length and saturation of the triacylglycerolacyl chain inside the LDs in muscle cells [162], but there were notable differences in the size and subcellular location of LDs between athletes and those with type 2 diabetes. While people with type 2 diabetes stored most of their lipids in fewer, but larger, LDs primarily in the subsarcolemmal (SS) area of type II muscle fibers, athletes stored the majority of their lipids in numerous, normally sized LDs in the intramyofibrillar (IMF) area of type I muscle fibers [163]. Notably, larger LDs in type 2 diabetic patients had longer acyl chains than normally sized LDs, which may indicate a potential link between larger LDs and the SS area and decreased insulin sensitivity. Therefore, these results provide new information on how to compare the LDs of muscle cells to determine insulin sensitivity [162]. 3. Using Raman spectroscopy in cellular lipids in the future The sensitivity, resolution, and mobility of the system might be significantly increased by using sophisticated and efficient methods that target the Raman microscopy hardware and software. By collecting stable and enhanced signals, the new nanomaterials and composites utilized as SERS substrates will make it easier to identify molecules at low concentrations [164]. TERS signals may be enhanced by improving probe forms and geometric structures, surface coatings, and probe materials [165]. Through the use of Raman, integrating super-resolution microscopy (including photoactivated localization microscopy (PALM)/sto-chastic optical reconstruction microscopy (STORM), stimulated emission depletion microscopy (STED), and structured illumination microscopy (SIM) could achieve nanometer-level resolution and surpass the limit of light diffraction [166]. For the broad range of Raman inclinical diagnosis and treatment, including the use of digital micromirror devices, micro-spectrometers, micro-lasers, as well as spectrum preprocessing software and modular design, a practical and easy-to-use operating system is also essential. The technology of Raman multimodal imaging is promising. overcomes the limits of solo Raman technology in terms of sensitivity, resolution, and particular molecular identification by integrating with other techniques to provide full information about analytes.

Indo-American Journal of Pharma and Bio Sciences
Vol. 21, Issue 3, Aug 2023

In addition to providing chemical composition information without the need for complex sample preparation, fluorescence microscopy and Raman spectroscopy enable the capture of high-resolution cellular structure images, allowing for a more precise identification of lipid components in particular cell substructures [68]. Furthermore, by locating Raman imaging in certain areas and assisting in the identification of the source of fluorescence signals, fluorescence microscopy may effectively reduce fluorescence interference with Raman signals. Ramanspectroscopy's limitations in lipid identification were overcome in metabolic research by combining it with MS, which allowed for the clear identification of intracellular lipid composition and distribution [167]. Combining Raman technology with time-resolved technologies and super-resolution microscopy will boost its signal intensities and temporal resolution for multidimensional, real-time monitoring of changes in cellular dynamics. An extensive Raman database will be created by Intel- combining it with other omics data. A Raman Database of 161 Inorganic Compounds [169] and the ASERS Database of 63 Metabolites [168] are two examples of recent Raman spectroscopy databases that are typically focused on a single range of chemical compounds, frequently contain limited spectra information for biological samples, and lack interoperability with other databases. In order to store and manage large datasets derived from Raman spectroscopy, future comprehensive databases could be constructed. For cellular lipidomics research, the database should include signals from different cell types and cells under different physiological conditions in addition to the fundamental Raman spectra of single lipid standards. Additionally, the correlation of Raman spectral data with lipidomics, genomics, and transcriptomics will facilitate a more convenient exploration of cellular metabolic processes and molecular mechanisms, which is especially important for studying diseases related to metabolism. Artificial intelligence (AI) development not only tackles AI algorithms can greatly increase the efficiency of Raman spectral data analysis, particularly when handling large-scale, high-throughput datasets. This overcomes the limitations of traditional Raman spectroscopy in data processing, signal-to-noise ratio, and dynamic experimental adjustments, but also broadens its application in clinical disease diagnosis and treatment. Patterns in disease-related Raman spectra have previously been effectively identified using machine learning methods [170]. Self-driven Ramanspectroscopy's development opens the door to automated sample preparation, data collection, and analysis, which lowers human error and boosts experimental effectiveness. AI's ability to automatically regulate variables like laser intensity and exposure duration improved the signal quality in the dynamic process of cellular metabolism. It is anticipated that AI models trained on high-throughput Raman spectrum data would develop into useful instruments for clinical illness detection and therapy. For the early identification of metabolic illnesses such as diabetes and cardiovascular ailments, a strict monitoring system for the metabolite spectra in blood and urine samples is helpful. However, in conjunction with genetic and metabolic data from the same patient, AI analysis of Raman spectrum signals will provide individualized diagnostic and therapy recommendations for a greater number of therapeutic outcomes. 4. Clinical Use of Raman Spectroscopy Additionally, disorders including skin tumors, lung cancer, breast cancer, cardiovascular diseases, and non-alcoholic fatty liver disease (NAFLD) might be identified using Raman spectroscopy [171]. Fiber-optic Raman spectroscopy and spectrum modeling were used in conjunction with a new approach to rapidly characterize lipid unsaturation and the amount of carotenoid in the PVAT around the IMA [172]. The Canadian Cardiovascular Society (CCS) Angina Grading Scale and the PVAT phenotype were strongly associated, and the PVAT could quickly evaluate transplanted IMAs in patients having coronary artery bypass surgery [172]. In vitro and in vivo, the image-guided Raman spectroscopic probe-tracking system based on white light/fluorescence pictures accurately defined tumor margins from healthy tissues, helping to remove tumor tissues completely while preserving as much healthy tissue as possible [173]. The simultaneous collection of biochemical and morphological data on skin tissues for the precise identification of skin tumors was made possible by the combination of portable Raman spectroscopic instruments with dermoscopy and computer-aided systems [174]. However, the intrinsically weak Raman signals make it difficult to quickly and non-invasively get high-quality signals in clinical samples, particularly in vivo [171]. They also necessitate the use of extremely

Indo-American Journal of Pharma and Bio Sciences

Vol. 21, Issue 3, Aug 2023

sensitive detectors and high-power laser sources, which raises the cost of equipment. In addition to articulating light delivery, the optical fibers in Raman systems also satisfy medical criteria for various clinical goals [175]. The complex chemical composition of biological samples and technical consistency across different laboratories remain major challenges for the clinical implementation of Raman. Variations in sample preparation procedures, such as fixation methods and tissue section thickness, could result in significant differences in spectral signals and potentially compromise diagnostic consistency.

Conclusions

Combining Raman spectroscopy with various imaging tools provides important non-invasive insights into cellular lipid metabolism, and sophisticated statistical methods and machine learning algorithms make it easier to analyze complicated Raman spectrum data. The limits of Raman are still there, however. Particularly for lipids at low concentrations or those that are widely distributed and resulted in attenuated Raman signals, the accuracy of detecting lipid species within complex tissue matrices is intrinsically constrained. The majority of conventional Raman spectroscopy techniques are usually only appropriate for revealing lipid compositions in bigger structures like LDs and cell membranes due to the limits of laser wavelength and weak signals from tiny structures. However, precise positioning, the removal of background interference, and high operational skills remain challenges for further in-depth study of intracellular organelles and their dynamic changes. Advanced techniques like SERS, TERS, and SRS improve Raman spatial resolution at the nanoscale and enable the discrimination of smaller organelles like mitochondria, lysosomes, and ER. Furthermore, there is still much to learn about quantitative analysis of lipids, even with the use of machine learning algorithms and signal deconvolution techniques.

References

[1] [1] R.A. DeBose-Boyd, Lipid metabolism: Significance and Regulation, Semin. Cell Dev. Biol. 81 (2018), 97. [2] ApoElipidation as a therapeutic target in Alzheimer's disease, M.F. Lamfranco, C.A. Ng, and G.W. Rebeck, Int. Mol, J. Science. 21 (2020), 6336.[3] X. The connection between lipid phytochemicals, obesity, and chronic illnesses associated with it, Food Function, Guo, T. Zhang, L. Shi, et al. 9 (2018) 6048–6062.

[4] Z. Wu, S. Thoro€e-Boveleth, G.I. Bagarolo, et al., "Lipidomics":Massspectro lipids' metric and chemometric analyses, Adv. Drug Delivery. 294–307 in Rev. 159 (2020).

[2] [5] M. Lange and M. Fedorova, Assessment of Accuracy in Lipid Quantification Using HILIC and RPLC MS on the Example of NIST® SRM®1950 Metabolites in Human Plasma, Anal. bioanal. chemical. 412, 3573–3584 (2020). [6] C. Immunofluorescence labeling of lipid-binding proteins CERTs to track lipid raft dynamics, Giovagnoni, S.M. Crivelli, M. Losen, et al., Methods Mol.Biol. 327e335 in 2187 (2021).

[7] H. Appelqvist,K. Stranius,K. Bo€rjesson,et al.,Specificimagingof intracellularlipid droplets using a benzothiadiazole derivative withsolvatochromicproperties, Bioconjug. chemical. (2017) 1363–1370, 28.

[8] N. Schieda, C.B. van der Pol, B. Moosavi, et al., Intracellular lipid in papillaryrenal cell carcinoma (pRCC): T2 weighted (T2W) MRI and pathologiccorre-lation, Eur. Radiol. 2134e2142, 25 (2015).

[9] J.C. Matuszczyk, G. Zijlstra, D. Ede, et al., Raman spectroscopyprovidesvaluable process insights for cell-derived and cellular products, Curr. Opin.Biotechnol. 81 (2023), 102937.

[10]U.P.Agarwal,1064nmFTRamanspectroscopyforinvestigationsofplantcellwallsandotherbiomassmaterials,Front.PlantSci.5(2014),490.

[11] F. Gao, L. Xu, Y. Zhang, et al., Analytical Raman studyfordiscriminantanalysisofdifferentanimal derivedfeedstuff:Understandingthe high correlation between Raman spectroscopy and lipid haracteristics,Food Chem. 240 (2018) 989e996. [12] F.C.C. Oliveira, C.R.R. Brand~ao, H.F. Ramalho, et al., Adulteration of diesel/biodiesel blends by vegetable oil as determined by uriertransform(FT)nearinfraredspectrometryandFT-Ramanspectroscopy,Anal.Chim.Acta587 (2007) 194e199. [13] B. Tołpa, W. Paja, E. Trojnar, et al.,

Indo-American Journal of Pharma and Bio Sciences

FT-Raman spectra in combination withmachine learning and multivariate analyses as a diagnostic tool inbraintumors, Nanomedicine 57 (2024), 102737. [14] M. Kluz-Barłowska, T. Kluz, W. Paja, et al., FT-Raman and FTIR spectroscopyas a tools showing marker of platinum-resistant phenomena inwomensuffering from ovarian cancer, Sci. Rep. 14 (2024), 11025. [15] B.Schrader,G. Baranovic_, S. Keller, et al., Micro and two-dimensional NIR FTRaman spectroscopy, Fresenius' J. Anal. Chem. 349 (1994) 4e10. [16] L. Kelbauskas, R. Shetty, B. Cao, et al., Optical computed tomographyforspatially isotropic four-dimensional imaging of live single cells, Sci. Adv. 3(2017), e1602580. [17] G.W. Auner, S.K. Koya, C. Huang, et al., Applications of Raman spectroscopy incancer diagnosis, Cancer Metastasis Rev. 37 (2018) 691e717. [18] C. Krafft, J. Popp, The many facets of Raman spectroscopy forbiomedicalanalysis, Anal. Bioanal. Chem. 407 (2015) 699e717.

[19] G.Qi,J.Wang,K.Ma,etal.,Label-freesingle-particlesurface-enhancedRaman spectroscopy detection of phosphatidylserine externalization on cellmembraneswithmultifunctionalmicron-nanocompositeprobes,Anal.Chem. 93 (2021) 2183e2190. [20] D. Zhu, Z. Wang, S. Zong, et al., Investigating the intracellular behaviors ofliposomal nanohybridsviaSERS: Insights into the influence of metalnano-particles, Theranostics 8 (2018) 941e954. [21] X.S. Zheng, I.J. Jahn, K. Weber, et al., Label-free SERS in biologicalandbiomedical applications: Recent progress, current challenges and opportu-nities,Spectrochim.ActaAMol.Biomol.Spectrosc.197(2018)56e77.

[22] A. Gall, A.A. Pascal, B. Robert, Vibrational techniques applied tophotosyn-thesis: Resonance Raman andfluorescence line-narrowing, Biochim. Bio-phys. Acta 1847 (2015) 12e18. [23] M. Ishigaki, P. Meksiarun, Y. Kitahama, et al., Unveiling the aggregation oflycopene in vitroand in vivo: UV-vis, resonance Raman, and Raman imagingstudies, J. Phys. Chem. B 121 (2017) 8046e8057.

[24] U.Blume-Peytavi,A.Rolland,M.E.Darvin,etal.,Cutaneouslycope neandbeta-carotene levels measured by resonance Raman spectroscopy:Highreliability and sensitivity to oral lactolycopene deprivation and supple-mentation, Eur. J. Pharm. Biopharm. 73 (2009) 187e194. [25] R.E. Kast, S.C. Tucker, K. Killian, et al., Emerging technology: ApplicationsofRaman spectroscopy for prostate cancer, Cancer Metastasis Rev. 33 (2014)673e693.

[26] D. MrCenovi´c, W. Ge, N. Kumar, et al., Nanoscale chemical imaging of humancell membranes using tip-enhanced Raman spectroscopy, Angew. Chem. Int. Ed61(2022),e202210288.

[27] P. Verma, Tip-enhanced Raman spectroscopy: Technique and recentad-vances, Chem. Rev. 117 (2017) 6447e6466.

[28]R.Bo€hme,M.Mkandawire,U.Krause-Buchholz,etal.,Characterizingcyto chrome c states: TERS studies of whole mitochondria, Chem.Commun.(Camb) 47 (2011) 11453e11455.

[29] N. Kumar, M.M. Drozdz, H. Jiang, et al., Nanoscale mapping of newly-syn-thesised phospholipid moleculesin a biological cell using tip-enhancedRaman spectroscopy, Chem. Commun. (Camb) 53 (2017) 2451e2454.

[30] T.Stepanenko,K.Sofin´ska,N.Wilkosz,etal.,Surface-enhancedRaman scattering (SERS) and tip-enhanced Raman scattering (TERS) in label-freecharacterization of erythrocyte membranes and extracellular vesicles at thenano-scale and molecular level, Analyst 149 (2024) 778e788.

[31] Y. Pandey, N. Kumar, G. Goubert, et al., Nanoscale chemical imagingofsupportedlipidmonolayersusingtip-enhancedRamanspectroscopy,Angew. Chem. Int. Ed 60 (2021) 19041e19046. [32] A. Folick, W. Min, M.C. Wang, Label-free imaging of lipid dynamicsusingCoherent Anti-stokes Raman Scattering (CARS) and Stimulated RamanScattering(SRS)microscopy,Curr.Opin.Genet.Dev.21(2011)585e590.

[33] C. Di Napoli, I. Pope, F. Masia, et al., Hyperspectral and differentialCARSmicroscopy for quantitative chemical imaging in human adipocytes, Biomed.Opt. Express 5 (2014) 1378e1390.

[34] J. Saarinen, E. So€zeri, S.J. Fraser-Miller, et al., Insights into Caco-2 cell culturestructure using coherent anti-Stokes Raman scattering (CARS) microscopy,Int. J. Pharm. 523 (2017) 270e280.

[35] L. Guo, J. Huang, Y. Chen, et al., Fiber-enhanced stimulated Raman scatteringand sensitive detection of dilute solutions, Biosensors (Basel) 12 (2022), 243. [36] M.C. Wang, W. Min, C.W. Freudiger, et al., RNAi screening for fatregulatorygeneswithSRSmicroscopy,Nat.Me

Indo-American Journal of Pharma and Bio Sciences

Vol. 21, Issue 3, Aug 2023

thods8(2011)135e138. [37] C.Cao,D.Zhou,T.Chen,etal.,Label-freedigitalquantificationoflipiddroplets in single cells by stimulated Raman microscopy on amicrofluidicplatform, Anal. Chem. 88 (2016) 4931e4939. [38]A.BorekDorosz,A.Pieczara,K.Czamara,etal., Whatistheabilityofinflamedendotheliumtoupta keexogenoussaturatedfattyacids? Aproof-of-concept study using spontaneous Raman, SRS and CARS microscopy, Cell.Mol. Life Sci. 79 (2022), 593. [39] R. Smith, K.L. Wright, L. Ashton, Raman spectroscopy: An evolving techniquefor live cell studies, Analyst 141 (2016) 3590e3600. [40] J.W. Chan, D.S. Taylor, D.L. Thompson, The effect of cellfixation onthediscrimination of normal and leukemia cells with laser tweezers Ramanspectroscopy, Biopolymers 91 (2009) 132e139. [41] S.M. Levchenko, X. Peng, L. Liu, et al., The impact of cellfixation on coherentanti-stokes Raman scattering signal intensity in neuronal and glial cell lines, J.Biophotonics12(2019),e201800203.
[42] C. Jüngst, M. Klein, A. Zumbusch, Long-term live cell microscopy studiesoflipid droplet fusion dynamics in adipocytes, J. Lipid Res. 54 (2013)3419e3429. [43] C. Zhang, S.A. Boppart, Tracking the formation and degradation of fatty-acid-accumulated mitochondria using label-free chemical imaging, Sci. Rep. 11(2021), 6671. [44] A. Zoladek, F. Pascut, P. Patel, et al., Development of Raman ImagingSystemfor time-course imaging of single living cells, Spectroscopy 24 (2010)131e136.
[45] E.Aboualizadeh,E.C.Mattson,C.L.O'Hara,etal.,Coldshockinducesapoptosis of dorsal root ganglion neurons plated on infrared windows,An-alyst 140 (2015) 4046e4056. [46] I.R. Suhito, Y. Han, J. Min, et al.,In situlabel-free monitoring of human adi-pose-derived mesenchymal stem cell differentiation into multiplelineages,Biomaterials 154 (2018) 223e233.
[47] M. Gargotti, E. Efeoglu, H.J. Byrne, et al., Raman spectroscopydetectsbiochemicalchangesdueto differentcellcultureenvironmentsinlivecellsin vitro, Anal. Bioanal. Chem. 410 (2018) 7537e7550. [48] Y. Tan, S.O. Konorov, H.G. Schulze, et al., Comparative study usingRamanmicrospectroscopy reveals spectral signatures of human induced pluripotentcells more closely resemble those from human embryonic stem cells thanthose from differentiated cells, Analyst 137 (2012) 4509e4515. [49] L. Yang, J. Motohisa, J. Takeda, et al., Selective-area growth ofhexagonalnanopillars with single InGaAs/GaAs quantum wells on GaAs(111)B sub-strate and their temperature-dependent photoluminescence, Nanotech-nology 18 (2007), 105302. [50] O. Ryabchykov, J. Popp, T. Bocklitz, Fusion of MALDI spectrometricimagingand Raman spectroscopic data for the analysis of biological samples, Front.Chem. 6 (2018), 257.
[51] V. Avilkina, D. Leterme, G. Falgayrac, et al., Severity level and duration ofenergy deficit in mice affect bone phenotype and bone marrow stromal celldifferentiation capacity, Front. Endocrinol. (Lausanne) 13 (2022), 880503.
[52] M.J. Hackett, J.B. Aitken, F. El-Assaad, et al., Mechanisms of murinecerebralmalaria: Multimodal imaging of altered cerebral metabolism and roteinoxidationathemorrhagesites,Sci.Adv.1(2015),e1500911.
[53] J. Marzi, E. Fuhrmann, E. Brauchle, et al., Non-invasive three-dimensional cellanalysis in bioinks by Raman imaging, ACS Appl. Mater. Interfaces 14 (2022)30455e30465.
[54] H.Salehi,A.Ramoji,S.Mougari,etal.,Specificintracellularsignatureof SARS-CoV-2 infection using confocal Raman microscopy, Commun. Chem. 5(2022), 85.
[55] S.K. Paidi, J.R. Troncoso, M.G. Harper, et al., Raman spectroscopy revealsphenotype switches in breast cancer metastasis, Theranostics 12(2022)5351e5363.
[56] H. Chi, S. Hu, D. Lin, Development of an automated Raman system and use ofprincipalcomponentanalysistoclassifyrealandcounterfeitliquors,RSCAdv. 13 (2023) 33288e33293.
[57] Y. Jin, H. Tian, Z. Gao, et al., Oil content analysis of corn seeds using a hand-held Raman spectrometer and spectral peak decomposition algorithm, Front.Plant Sci. 14 (2023), 1174747.
[58] Anu, A. Srivastava, M.S. Khan, Principle component analysis fornonlinearoptical properties of thiophene-based metal

Indo-American Journal of Pharma and Bio Sciences
Vol. 21 Issue 3, Aug 2023

complexes, J. Mol. Model. 27(2021), 340.
[59] M. Bonsignore, S. Trusso, C. De Pasquale, et al., A multivariate analysis ofMultiple Myeloma subtype plasma cells, Spectrochim. Acta A Mol.Biomol.Spectrosc. 258 (2021), 119813.
[60] Y. Shao, H. Fang, H. Zhou, et al., Detection and imaging of lipids of Scene-desmus obliquusbased on confocal Raman microspectroscopy,Biotechnol.Biofuels 10 (2017), 300.
[61] H. Xin, J. Zhang, C. Yang, et al., Direct detection of inhomogeneity in CVD-grown 2D TMD materialsviaK-means clustering Raman analysis,Nano-materials (Basel) 12 (2022), 414.
[62] I.W.Schie,T.Huser,MethodsandapplicationsofRamanmicrospectroscopyto single-cell analysis, Appl. Spectrosc. 67 (2013) 813e828.
[63] E.W. Hislop, W.J. Tipping, K. Faulds, et al., Label-free imaging of lipid dropletsin prostate cells using stimulated Raman scattering microscopy and multi-variate analysis, Anal. Chem. 94 (2022) 8899e8908.
[64] G.I. Petrov, R. Arora, V.V. Yakovlev, Coherent anti-Stokes Ramanscatteringimaging of microcalcifications associated with breast cancer, Analyst 146(2021) 1253e1259.
[65] M.Ishigaki,H.Hitomi,Y. Ozaki,et al.,Exposingintracellularmolecularchanges during the differentiation of human-induced pluripotent stem cellsinto erythropoietin-producing cells using Raman spectroscopy and imaging,Sci. Rep. 12 (2022), 20454.
[66] N. Su, S. Weng, L. Wang, et al., Reflectance spectroscopy withmultivariatemethods for non-destructive discrimination of edible oil adulteration, Bio-sensors (Basel) 11 (2021), 492.
[67] S.K. Paidi, P.M. Diaz, S. Dadgar, et al., Label-free Raman spectroscopy revealssignatures of radiation resistance in the tumor microenvironment,CancerRes. 79 (2019) 2054e2064.
[68] A. Adamczyk, A.M. Nowakowska, J. Jakubowska, et al., Raman classification ofselected subtypes of acute lymphoblastic leukemia (ALL), Analyst 149 (2024)571e581.
[69] K. Czamara, K. Majzner, M.Z. Pacia, et al., Raman spectroscopy of lipids:Areview, J. Raman Spectrosc. 46 (2015) 4e20.
[70] Y. Xu, X. Hou, Q. Zhu, et al., Phenotype identification of HeLa cells knockoutCDK6 gene based on label-free Raman imaging, Anal. Chem. 94 (2022)8890e8898.
[71] E. Stanek, M.Z. Pacia, A. Kaczor, et al., The distinct phenotype of primary adi-pocytes and adipocytes derived from stem cells of white adipose tissue asassessedbyRamanandfluorescenceimaging,Cell.Mol.LifeSci.79(2022),383.
[72] N. Dahdah, A. Gonzalez-Franquesa, S. Samino, et al., Effects oflifestyleintervention in tissue-specific lipidomic profile of formerly obese mice, Int. J.Mol. Sci. 22 (2021), 3694.
[73] R. Basson, C. Lima, H. Muhamadali, et al., Assessment of transdermal deliveryof topical compounds in skin scarring using a novel combined approachofRaman spectroscopy and high-performance liquid chromatography, Adv.Wound Care (New Rochelle) 10 (2021) 1e12.
[74] K.J.Lee,G.E.Ji,Free-fatty-acid-regulatingeffectsoffermentedredginsengare mediated by hormones and by the autonomic nervous system, J. GinsengRes. 38 (2014) 97e105.
[75] S.Bresson,M.ElMarssi,B.Khelifa,Ramanspectroscopyinvestigationofvarioussaturated monoacid triglycerides, Chem. Phys. Lipids 134 (2005) 119e129.
[76] O.Samek,A.Jona´s,Z.Pila´t,etal.,Ramanmicrospectroscopyofindividual algal cells: Sensing unsaturation of storage lipidsin vivo, Sensors (Basel)10(2010) 8635e8651.
[77] Y. Nojima, T. Takaya, K. Iwata, Energy transfer characteristics of lipid bilayermembranes of liposomes examined with picosecond time-resolvedRamanspectroscopy, J. Phys. Chem. B 127 (2023) 6684e6693.
[78] E. Bik, N. Mielniczek, M. Jarosz, et al., Tunicamycin inducedendoplasmicreticulumchangesinendothelialcellsinvestigatedinvitrobyconfocalRaman imaging, Analyst 144 (2019) 6561e6569.
[79] C. Krafft, L. Neudert, T. Simat, et al., Near infrared Raman spectra ofhumanbrain lipids, Spectrochim. Acta A Mol. Biomol. Spectrosc. 61 (2005)1529e1535.
[80] L.J. Dolch, C. Rak, G. Perin, et al., A palmitic acid elongase affects eicosa-pentaenoic acid and plastidial monogalactosyldiacylglycerol levels inNan-

Indo-American Journal of Pharma and Bio Sciences

Vol. 21, Issue 3, Aug 2023

nochloropsis, Plant Physiol. 173 (2017) 742e759. [81] K. Shirota, K. Yagi, T. Inaba, et al., Detection of sphingomyelin clusters byRaman spectroscopy, Biophys. J. 111 (2016) 999e1007. [82] X. Liu, S. Guo, T. Bocklitz, et al., Nondestructive 3D imaging and quantification of hydrated biofilm matrix by confocal Raman microscopy coupled withnon-negative matrix factorization, Water Res. 210 (2022), 117973. [83] J. Zhang, Q. Li, Y. Wu, et al., Cholesterol content in cell membrane maintainssurface levels of ErbB2 and confers a therapeutic vulnerability inErbB2-positivebreastcancer,CellCommun.Signal.17(2019),15.

[3]